Untargeted metabolomic analysis of the yeast lipin phosphatidate phosphatase (Pah1p) deletion using Isotopic Ratio Outlier Analysis (IROA) and LC-HRMS

Yu-Hsuan Tsai;[1] Timothy J. Garrett;[2] Yunping Qiu;[3] Robyn Moir;[5] Ian Willis;[5] Chris Beecher;[4] Richard A. Yost;[1,2] Irwin Kurland[3]

Department of Chemistry, University of Florida, Gainesville, FL;[1] Department of Pathology, Immunology, and Laboratory Medicine, University of Florida, Gainesville, FL;[2] Department of Medicine, Albert Einstein College of Medicine, Bronx, NY;[3] IROA Technologies, Ann Arbor, Michigan;[4] Department of Biochemistry, Albert Einstein College of Medicine, Bronx, NY.[5]



Overview:

- ***PAH1* knockout yeast was investigated for its effect on metabolome**
- **Isotopic Ratio Outlier Analysis (IROA) and Liquid chromatography high resolution mass spectrometry LC-HRMS) were used for the analysis**
- **Higher abundance of metabolites involved in the TCA cycle were observed from the knockout, suggest possibility of enhanced TCA cycle activity**

Introduction

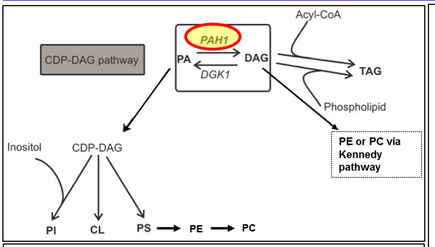


Figure 1. Phosphatidate phosphatase 1 (PAH1) and its regulating pathway, adapted from Guerfal et al.[1] PA, phosphatidic acid; DAG, diacylglyceride; DGK1, diacylclyceride kinase 1; TAG, triacylglyceride, PI, phosphatidylinositol; CL cardiolipin; PS, phosphatidyl-serine; PE, phosphatidylethanolamine; PC, phosphatidylcholine.

Lipins are phosphatidate phosphatases that generate diacylglycerol (DAG) from phosphatidic acid (PA), regulating a pathway key for production of triglycerides (PA->DAG->TAG). Absence of the mammalian lipin results in lipodystrophy, and yeast lipin (Pah1p) controls the formation of cytosolic lipid droplets. Depletion of PAH1 (*pah1*Δ) has been shown to result in a dramatic decrease in lipid droplet number. Metabolic pathways that might mediate this effect, and possibly have relevance to mammalian lipin-dependent lipodystrophy, were examined using Isotopic Ratio Outlier Analysis (IROA). IROA is a mass spectrometry-based metabolomic profiling method using ^{13}C labeling to eliminate sample-to-sample variance, discriminate against noise and artifacts, and improve compound identification. This work utilized IROA with LC-HRMS and investigated the metabolomic profiles from WT yeast vs *pah1*Δ.

IROA

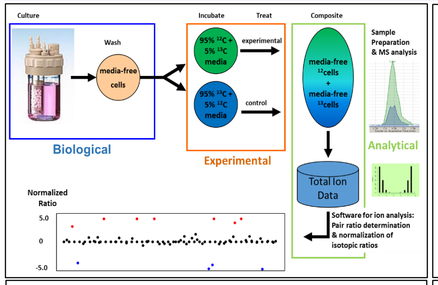


Figure 2. IROA workflow representation

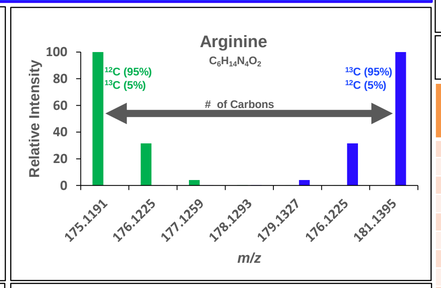


Figure 3. Representation of IROA pattern calculated using arginine

Methods

Wild-type (WT) and *pah1*Δ::natR (KO) CEN.PK yeast strains were grown to mid log phase on Yeast Nitrogen Base without amino acids, containing either 5% or 95%^{13}C glucose. Cells were harvested by vacuum filtration, washed with distilled water, and metabolism quenched at -20° C in 4:4:2 (v:v:v) methanol:acetonitrile:water. The internal standards, 10 µL of 2 mM of chlorophenylalanine in water and 5 µL of 10mM cholesterol in methanol, were spiked into the yeast suspensions (approximately 2.0×10^8 cells) before glass bead breakage and clarification by centrifugation at 4° C. Extracts were analyzed by LC-HRMS using a Thermo Q Exactive in positive and negative ion modes with an ACE Excel 2 C18-PFP column (100×2.1 mm, 2 µm). Mobile phase A was water with 0.1% formic acid, whereas B was acetonitrile. The chromatography was performed at a flow rate of 0.350 mL/min following the gradient elution. The gradient profile was 100% A for 3 minutes , increased to 90% B in 10 minutes, held isocratic at 90% B for 3 minutes, then returned to initial conditions in 0.5 minutes, and equilibrated for 3 minutes. Heated electrospray (HESI) was used for both positive and negative ion mode analyses and was set at 3.5 kV and 350 °C. The heated capillary set at 300 °C, sheath gas at 30 (arbitrary unit, a.u.) and the auxiliary gas at 5 a.u. The mass spectrometer was set to scan from *m/z* 100 to *m/z* 1000 with a resolution of 70,000 at *m/z* 200. The raw data files were converted to mzXML for processing using two separate methods. First, triplicates of ^{12}C KO extracts and ^{12}C WT were compared. Peak picking was performed using XCMS using the R package, the extracted features were analyzed using the online web server MetaboAnalyst (http://www.metaboanalyst.ca). Significant features extracted using principal component analysis (PCA) were submitted to database search for potential identification. For signal response comparison, peak area of ions of interest were generated by batch analysis using QuanBrowser by Thermo. In addition, the analysis of a set of triplicates of 12C KO and 13C WT mixtures was performed in parallel using the Cluster Finder software built for IROA experiments. The identification of compounds was achieved by matching the signal response (e.g., *m/z* values of 12C and 13C and corresponding IROA pattern) with the built-in database in Cluster Finder.

Results

95% ^{12}C WT vs 95% ^{12}C KO, non-IROA

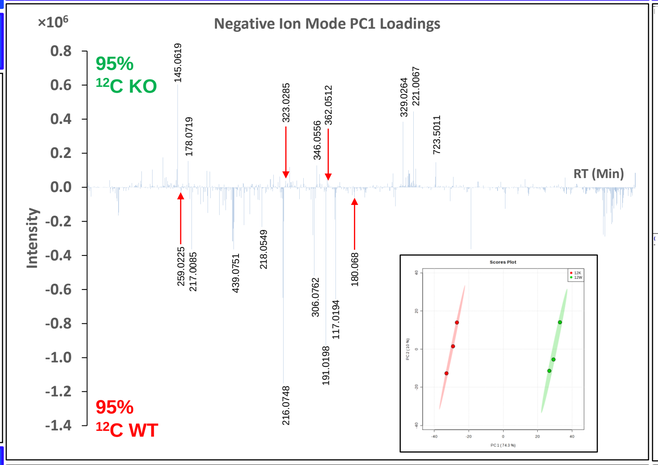


Figure 4. Principal component analysis (PCA) 2D scores plot of principal component 2 (PC2) vs PC1, and PC1 loadings plots generated from negative ion mode dataset of 95% ^{12}C labeled WT and 95% ^{12}C labeled KO.

5% ^{13}C KO vs 95% ^{13}C WT, IROA

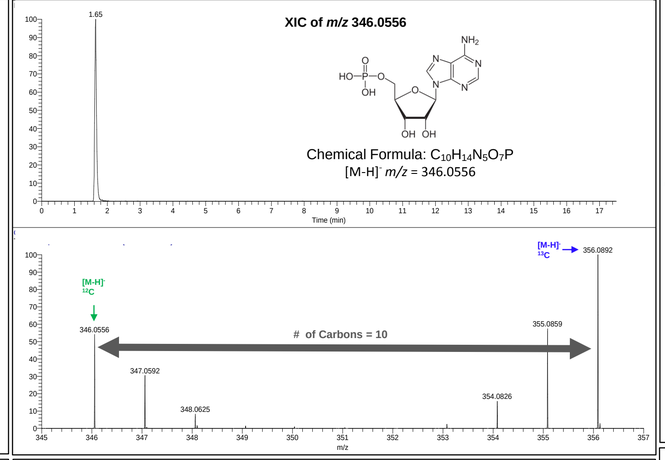


Figure 5. Extracted ion chromatogram (XIC) of *m/z* 346.0556 and averaged mass spectrum. *m/z* 346.0556 was identified as adenosine monophosphate by Cluster Finder based on the accurate mass and the IROA envelope.

Table 1. Significant compounds characterized with IROA envelopes, identified, and mass peak ratios extracted by Cluster Finder. The ratio between the ^{12}C and ^{13}C mass peaks were calculated; for ratios less than 1, $^{13}C/^{12}C$ ratio was also calculated for ease of comparison.†

Identification	Chemical Formula	^{12}C m/z Exact Mass	^{12}C m/z Accurate Mass	Mass Accuracy (ppm)	^{13}C m/z Exact Mass	^{13}C m/z Accurate Mass	Mass Accuracy (ppm)	RT (Min)	Mass Peaks $^{12}C/^{13}C$ Ave	STDEV	$1/[^{12}C/^{13}C]$†	KO relative to WT
Uridine monophosphate	$C_9H_{13}N_2O_9P$	323.0286	323.0285	-0.3	332.0588	332.0592	1.1	1.25	0.5	0.003	2.2	↓
Adenosine monophosphate	$C_{10}H_{14}N_5O_7P$	346.0558	346.0556	-0.8	356.0894	356.0896	0.8	1.64	0.5	0.02	1.9	↓
Cytosene monophosphate	$C_9H_{14}N_3O_8P$	322.0446	322.0448	0.8	331.0748	331.0752	1.4	1.07	0.5	0.02	1.9	↓
Guanosine monophosphate	$C_{10}H_{14}N_5O_8P$	362.0507	362.0512	1.2	372.0843	372.0842	-0.3	1.87	0.6	0.03	1.8	↓
Glutamine	$C_5H_{10}N_2O_3$	145.0619	145.0619	0.3	150.0786	150.0787	0.3	0.76	0.8	0.04	1.3	↓
Methionine	$C_5H_{11}NO_2S$	148.0438	148.0438	0.1	153.0606	153.0606	0.2	1.47	0.8	0.08	1.2	↓
Valine	$C_5H_{11}NO_2$	116.0717	116.0719	1.8	121.0885	121.0887	1.4	1.19	0.8	0.04	1.2	↓
Aspartate	$C_4H_7NO_4$	132.0302	132.0302	0.1	136.0437	136.0438	0.7	0.75	1.3	0.09		↑
Alanine	$C_3H_7NO_2$	88.0404	88.0406	1.7	91.0505	91.0507	2.1	0.76	1.3	0.08		↑
Ornithine	$C_5H_{12}N_2O_2$	131.0826	131.0826	0.1	136.0994	136.0995	0.9	0.81	1.3	0.09		↑
Asparagine	$C_4H_8N_2O_3$	131.0462	131.0463	0.3	135.0596	135.0598	1.4	0.74	1.4	0.08		↑
Inosine	$C_{10}H_{12}N_4O_5$	267.0735	267.0738	1.0	277.1070	277.1072	0.6	5.43	1.4	0.08		↑
Citrulline	$C_6H_{13}N_3O_3$	174.0884	174.0885	0.3	180.1085	180.1086	0.5	0.81	1.4	0.06		↑
Phosphoenolpyruvate	$C_3H_5O_6P$	166.9751	166.9752	0.6	169.9852	169.9854	1.1	0.86	1.4	0.05		↑
Tryptophan	$C_{11}H_{12}N_2O_2$	203.0826	203.0827	0.3	214.1195	214.1197	0.8	6.42	1.5	0.2		↑
Pyruvate	$C_3H_4O_3$	87.0088	87.0089	1.7	90.0188	90.0191	3.0	1.05	1.6	0.1		↑
Phenylalanine	$C_9H_{11}NO_2$	164.0717	164.0719	0.9	173.1019	173.1019	-0.2	5.59	1.6	0.1		↑
Aspartate semialdehyde	$C_4H_7NO_3$	116.0353	116.0355	1.7	120.0487	120.0488	0.2	1.26	1.6	0.0		↑
Ribose monophosphate	$C_5H_{11}O_8P$	229.0119	229.0121	1.0	234.0287	234.0289	1.0	0.77	1.9	0.1		↑
Adenisine diphosphate	$C_{10}H_{15}N_5O_{10}P_2$	426.0221	426.0224	0.5	436.0557	436.0562	1.2	1.35	1.9	0.1		↑
Malate	$C_4H_6O_5$	133.0142	133.0144	0.8	137.0277	137.0276	-0.5	1.09	2.7	0.1		↑
3-phosphoglycerate	$C_3H_7O_7P$	184.9857	184.9859	1.1	187.9957	187.9958	0.4	0.80	2.8	0.3		↑
Glycerol-3-phosphate	$C_3H_9O_6P$	171.0064	171.0065	0.7	174.0165	174.0167	1.5	0.77	2.9	0.1		↑
Tyrosine	$C_9H_{11}NO_3$	180.0666	180.0668	1.0	189.0968	189.0968	0.1	3.13	3.2	0.1		↑
Citrate	$C_6H_8O_7$	191.0197	191.0198	0.4	197.0399	197.0397	-0.7	1.84	3.7	0.1		↑
Fructose monophosphate	$C_6H_{13}O_9P$	259.0224	259.0225	0.1	265.0426	265.0424	-0.7	0.77	4.6	0.9		↑
Nicotinamide Adenine Dinucleotide	$C_{21}H_{27}N_7O_{14}P_2$	662.1019	662.1026	1.1	683.1723	683.1714	-1.4	3.15	4.9	0.4		↑
Succinate	$C_4H_6O_4$	117.0193	117.0194	0.6	121.0328	121.0328	0.0	2.21	5.4	0.3		↑
Glycerate	$C_3H_6O_4$	105.0193	105.0196	2.6	108.0294	108.0297	2.4	0.88	18.8	1.2		↑
Glucosamine monophosphate	$C_6H_{14}NO_8P$	258.0384	258.0385	0.3	264.0586	264.0582	-1.3	0.76	20.4	3.6		↑
Glycero-3-phosphoethanolamine	$C_5H_{14}NO_6P$	214.0486	214.0488	1.0	219.0654	219.0652	-0.8	0.77	20.8	4.0		↑
CDP-ethanolamine	$C_{11}H_{20}N_4O_{11}P_2$	445.0531	445.0536	1.1	456.0900	456.0905	1.1	0.88	142.7	4.5		↑

Summary and Future Work

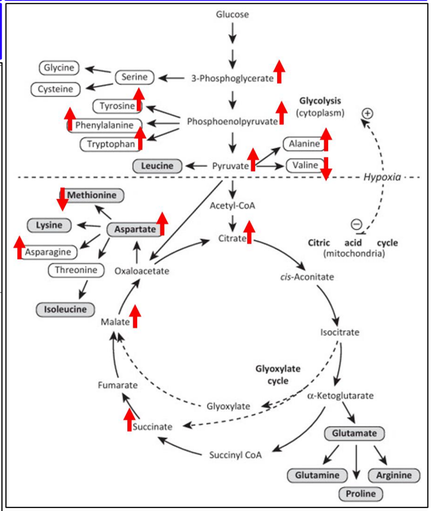


Figure 6. The tricarboxylic acid (TCA) cycle and metabolites observed with higher intensity in KO in this study; figure adapted from Eswarappa[2].

In this study, amino acid such as tyrosine, phenylalanine, and tryptophan responses were higher in the KO compared to the WT. Other metabolites involved in the TCA cycles, such as citrate and succinate, were also found higher in abundance in the KO compared to the WT. The observations suggest a potential increase in the TCA cycle activity. In a study performed by Guerfal et al., an enhanced protein production in *PAH1* depleted cells was observed; this observation could be related to the higher abundance of amino acids found in this current study. Other molecules such as adenosine diphosphate, cytosine monophosphate, and uridine monophosphate were found to be lower in the KO, suggesting that the purine and pyrimidine metabolic pathways could also be influenced. The large increases seen in *pah1*Δ phospholipids such as the 20-fold increase in glycero-3-phosphoethanolamine and the 140-fold increase in CDP-ethanolamine may be facilitated by the general increase in glycolysis and TCA cycle flux, redirected to phospholipid synthesis. *PAH1* controls the conversion of PA to other lipids such as DAGs, TAGs, PCs, and PEs, so analysis of the lipidome could provide valuable insight.

Acknowledgments

The authors would like to thank the National Institute of Health (NIH), the Clinical and Translational Science Institute (CTSI, UL1 TR000064), and Southeast Center for Integrated Metabolomics (SECIM) for financial support (NIH grant #U24 DK097209).

References

1. Guerfal, M.; Claes, K.; Knittelfelder, O.; De Rycke, R.; Kohlwein, S. D.; Callewaert, N., *Microbial Cell Factories* **2013,** *12*, 122-122.
2. Eswarappa, S. M.; Fox, P. L., *Trends in Biochemical Sciences* **1996,** *38* (5), 222-228.